J. Fluid Mech. (1991), *vol.* 224, *pp.* 335–359
Printed in Great Britain

Natural convection in a mushy layer

By M. GRAE WORSTER

Department of Engineering Sciences & Applied Mathematics *and* Department of Chemical Engineering, Northwestern University, Evanston, IL 60208, USA

(Received 2 January 1990 and in revised form 9 August 1990)

Governing equations for a mushy layer are analysed in the asymptotic regime $R_m \gg 1$, where R_m is an appropriately defined Rayleigh number. A model is proposed in which there is downward flow everywhere in the mushy layer except in and near localized chimneys, which are characterized by having zero solid fraction. Upward, convective flow within the chimneys is driven by compositional buoyancy. The radius of each chimney is determined locally by thermal balances within a boundary layer that surrounds it. Simple solutions are derived to determine the structure of the mushy layer away from the immediate vicinity of chimneys in order to demonstrate the gross effects of convection upon the solidification within the layer.

1. Introduction

The internal structure of an alloy depends crucially upon the history of its solidification from a melt. For example, the geometry of the melt region, the rate of solidification, and fluid motions in the melt all affect the solidified product. These properties are all determined by internal processes that occur in response to external conditions such as the shape of the container and the location of cooled boundaries, the degree of cooling, the initial concentration of the melt, and the existence of body forces such as those produced by gravitational or magnetic fields. For example, when solidification takes place in a gravitational field, natural convective flow of the melt can be driven by thermal gradients that are set up by the imposed cooling, or by compositional gradients that are generated when one component of the alloy is preferentially incorporated within the growing solid, or by both.

A phenomenon that occurs commonly during the solidification of alloys is the formation of partially solidified regions called mushy zones or mushy layers. These often take the form of a forest of solid, dendritic crystals, oriented principally along the direction of strongest thermal gradient, with fluid filling the interstices (figure 1). If the fluid flows through the interstices of a mushy layer, the transport of both heat and solute is altered and can cause additional growth of the dendrites or cause them to dissolve. Thus there are complex interactions between fluid flow and solidification in which density gradients generated by solidification drive a flow that can in turn modify the rates and structure of the crystal growth. Conversely, the growth and dissolution of dendrites, induced by convection, alters the permeability of the mushy layer viewed as a porous medium, which changes the pattern of convection.

The interactions that occur in a gravitational field depend strongly upon the direction of solidification relative to gravity. For the simple geometries in which a melt is cooled from a single, flat, horizontal surface, Huppert & Worster (1985) identified six different regimes distinguished by whether the surface forms an upper or a lower boundary of the melt and whether the density of the melt is increased, decreased or remains constant when the melt is depleted of the component forming

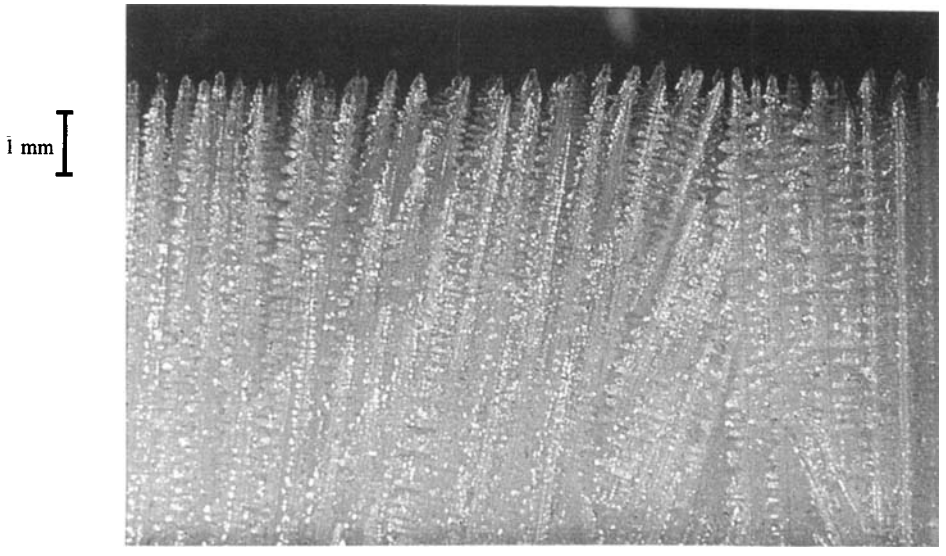

FIGURE 1. A mushy layer of ammonium chloride crystals formed by cooling an aqueous solution of ammonium chloride from below. The millimetre scale on the left shows that the typical spacing between crystals is very small compared with the depth of the mushy layer, which was about 7 cm when the photograph was taken. The photograph is reproduced courtesy of H. E. Huppert.

the solid phase. Several of these cases have since been elucidated by combined laboratory investigations and mathematical analyses of simple models (Huppert & Worster 1985; Worster 1986; Turner, Huppert & Sparks 1986; Kerr *et al.* 1989, 1990*a*, *b*, *c*). In all of these earlier studies, the compositional density field that is generated is stable and there is either no mushy layer or the fluid in the mushy layer is stagnant.

Woods & Huppert (1989) considered the solidification from below of a two-component melt that becomes buoyant once it is depleted of the component forming the solid phase. In such a case, the vertical variation of temperature causes a statically stable density field, while the compositionally induced density variations are convectively unstable. Woods & Huppert investigated the growth of a planar solidification front, and showed how its rate of advance depends upon the interaction of the compositionally driven flow in the overlying melt with the stable thermal boundary layer. In this paper, we shall be concerned additionally with the growth of a mushy layer, where two different modes of convection can occur. In the liquid ahead of the mush–liquid interface there is a compositional boundary layer that is potentially unstable. The compositional variation across this boundary layer is much smaller than typically exists ahead of a plane solidification front, so we shall argue that double-diffusive, finger convection is more likely to occur than the wholescale disruption of the stable thermal boundary layer suggested by Woods & Huppert. The second mode of convection involves the escape of buoyant, interstitial fluid from the mushy layer into the overlying liquid region. It is the means of escape that is particularly intriguing and provides a focus for this study.

Copley *et al.* (1970) reported experiments in which they had cooled and crystallized from below aqueous solutions of ammonium chloride. This particular salt was chosen because its crystal habit is similar to that of many metallic alloys. The authors found that convection of buoyant fluid from the interstices of the mushy layer, which

formed as crystals of ammonium chloride grew at the base of the container, took the form of narrow, vertical plumes rising through crystal-free vents or 'chimneys' in the dendritic matrix. They suggested that these convectively formed chimneys are the cause of the 'freckles' that are observed in completely solidified ingots. Freckles are imperfections that interrupt the uniformity of the microstructure of a casting, causing areas of mechanical weakness.

There have been some attempts to understand the origin of freckles in terms of the convective instabilities that lead to chimney formation (e.g. Fowler 1985). Our aim in this paper, however, is to understand the nature of the flow and the structure of the mushy layer that occurs once chimneys are fully developed. Some aspects of the flow structure have been analysed previously by Roberts & Loper (1983) but they did not include the thermodynamic interactions between the flow and the growth of solid within the mushy layer; interactions that are fundamental to the overall behaviour of the system.

A concurrent aim is to provide analytical solutions to equations that govern the evolution of an 'ideal' mushy layer that include the effects of gravitationally driven convection. Sets of governing equations have been proposed by Hills, Loper & Roberts (1983), based on principles of diffusive mixture theory, and independently by Worster (1986) based upon simple considerations of local heat and mass balances. Both sets are derived with many assumptions about the nature of crystal growth within a mushy layer and can be thought of as providing definitions of an 'ideal' mushy layer. It remains to be seen whether the proposed equations are adequate to describe any of the formations that are observed experimentally or, alternatively, whether any physical system can be treated as being 'ideal'. To date, these equations have been solved and compared to experimental data only for cases in which there is no flow of the interstitial fluid. It is hoped that the theoretical results of this paper, in which the full interactions between fluid flow and crystal growth are taken into account, will provide a basis for comparison with future experimental investigations.

The mathematical equations governing the evolution of an 'ideal' mushy layer are presented in §2. Analytical solutions for cases with no fluid flow are given in §3 in order to quantify the destabilizing influence of compositional buoyancy relative to the stabilizing influence of thermal buoyancy in different regions of the system. This competition is discussed in §4. In particular, a single Rayleigh number R_m is identified for the mushy layer, where the temperature and composition of the liquid are coupled. Consideration of the physical balances expressed by R_m gives a hint as to the likely structure of a convecting mushy layer. This structure is further elucidated in §5, in which fully developed convection is analysed by seeking solutions in the asymptotic regime $R_m \gg 1$. The analysis of §5 also provides estimates of the convective fluxes of fluid, heat and solute through an individual chimney. This analysis allows us, in §6, to determine how the depth of the mushy layer and the solid fraction within it vary as the strength of convection increases. In §7 we discuss how the present results might apply to experimental systems and how the number density of chimneys might be determined, which would allow calculations to be made of the total convective exchanges between the mushy layer and the overlying liquid region.

2. Equations governing a mushy layer

Many previous authors have presented equations governing the internal evolution of mushy zones (e.g. Flemings 1981; Hills *et al.* 1983; Fowler 1985). The formulation presented here follows most closely the approach of Worster (1986). In all these

formulations, appeal is made to the fine-scale internal structure of the mushy region in order to treat it thermodynamically as a single continuum phase. The temperature T and the composition of the interstitial liquid C are assumed to be uniform over lengthscales typical of the interdendritic spacing. Then differential equations describing conservation of heat and solute can be written as

$$c_{\mathrm{m}}\frac{\partial T}{\partial t}+c_{\mathrm{l}}\,\boldsymbol{U}\cdot\boldsymbol{\nabla}T=\boldsymbol{\nabla}\cdot(k_{\mathrm{m}}\,\boldsymbol{\nabla}T)+\mathscr{L}_{\mathrm{s}}\frac{\partial\phi}{\partial t}, \tag{2.1a}$$

$$(1-\phi)\frac{\partial C}{\partial t}+\boldsymbol{U}\cdot\boldsymbol{\nabla}C=\boldsymbol{\nabla}\cdot(D_{\mathrm{m}}\,\boldsymbol{\nabla}C)+(C-C_{\mathrm{s}})\frac{\partial\phi}{\partial t}, \tag{2.1b}$$

if we assume that there is no expansion of contraction upon changes of phase. The physical parameters in these equations are the specific heat per unit volume c, the latent heat of solidification per unit volume $\mathscr{L}$, the thermal conductivity k and the solutal diffusivity D, where subscripts 's', 'l' and 'm' denote properties of the solid, liquid and mushy phases respectively. The volume fraction of solid dendrites, of uniform composition C_{s}, is denoted by ϕ. The specific heat per unit volume of the mushy phase is given by

$$c_{\mathrm{m}}=\phi c_{\mathrm{s}}+(1-\phi)\,c_{\mathrm{l}}, \tag{2.2}$$

and it is assumed that the molecular transport processes are given by similar volume-fraction weighted averages

$$k_{\mathrm{m}}=\phi k_{\mathrm{s}}+(1-\phi)\,k_{\mathrm{l}}, \tag{2.3}$$

$$D_{\mathrm{m}}=(1-\phi)\,D_{\mathrm{l}}, \tag{2.4}$$

having ignored chemical diffusion in the solid phase. Expressions (2.3) and (2.4) are only approximate, since such transport coefficients should generally depend upon the internal morphology of the two-phase medium (Batchelor 1974), but these expressions have been found to lead to good agreement with the results of laboratory experiments on stagnant mushy layers (Huppert & Worster 1985; Worster 1986; Kerr *et al.* 1989, 1990*a*,*b*,*c*).

Since we have ignored volume changes upon change of phase, the continuity equation takes the form

$$\boldsymbol{\nabla}\cdot\boldsymbol{U}=0, \tag{2.5}$$

satisfied by the volume flux of interdendritic fluid $\boldsymbol{U}=(1-\phi)\,\boldsymbol{u}$, where $\boldsymbol{u}$ is the local fluid velocity.

A fundamentally important feature of our model of mushy regions is the coupling of the temperature and concentration fields through the source terms, proportional to $\partial\phi/\partial t$, on the right-hand sides of (2.1). Physically, these represent the latent heat and solvent that are released as freezing or melting takes place within the mushy layer. The rate of change of ϕ is determined indirectly by assuming that the internal freezing or melting is sufficiently rapid that the mushy layer is kept in local thermodynamic equilibrium according to the phase diagram illustrated in figure 2(*a*). Thus the temperature and composition are required to satisfy the liquidus relationship $T=T_{\mathrm{L}}(C)$, which we approximate here by the linear expression

$$T=T_{\mathrm{L}}(C_0)+\Gamma(C-C_0), \tag{2.6}$$

where C_0 is a reference value of the composition of the liquid and Γ is the slope of the liquidus curve at $C=C_0$, which is taken to be positive.

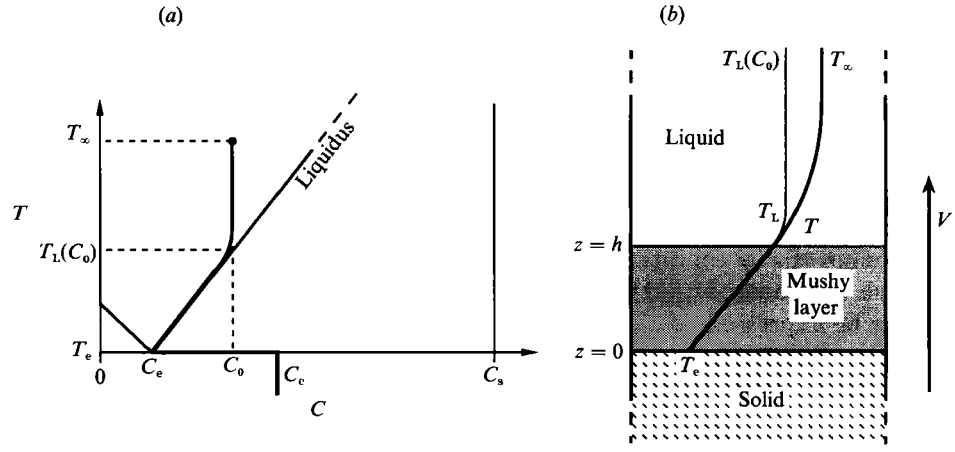

FIGURE 2. (*a*) The equilibrium phase diagram used in the theoretical model. It is a binary, eutectic phase diagram with end-member concentrations $C = 0$ and $C = C_s$. The two solidus curves are assumed to be vertical, i.e. the segregation coefficient is taken to be zero, and the liquidus curve is linear. With the convention that the density of the melt increases with C, the initial concentration C_0 is taken to be greater than the eutectic concentration C_e. In steady states, the concentration C_c of the composite solid that forms below the eutectic temperature T_e is equal to C_0 if there is no (convective) macrosegregation but is typically greater than C_0 once compositional convection transports solvent vertically to $z = +\infty$. (*b*) A schematic diagram of the solidification process that is being modelled. The system is steady in a frame moving with the prescribed solidification speed V. A mushy layer lies above a completely solid region, where the temperature is below the eutectic temperature, and below a completely liquid region. The temperature profile T is shown together with the profile of the local liquidus temperature $T_L(C)$.

The interior description of the mushy layer is completed with a dynamical equation governing the fluid flow. Consistent with the view of the mushy layer as a porous medium, we follow Roberts & Loper (1983) and Fowler (1985) by adopting Darcy's equation

$$\frac{\mu \boldsymbol{U}}{\Pi} = -\nabla p + (\rho_l - \rho_0)\boldsymbol{g}, \tag{2.7}$$

where μ is the dynamic viscosity of the liquid, p is the pressure, $\boldsymbol{g}$ is the acceleration due to gravity, ρ_0 is some reference value of the fluid density and Π is the permeability of the mushy layer. In general, a constitutive equation

$$\Pi = \Pi(\chi) \tag{2.8}$$

is required to relate the permeability Π to the local liquid fraction $\chi = 1 - \phi$. We do not need an explicit form for the constitutive equation in this paper, since we shall only be concerned with asymptotic states in which the left-hand side of (2.7) can be neglected to leading order. However, we shall make important, implicit use of the fact that the permeability increases as the solid fraction decreases. To determine the buoyancy forcing (2.7), the density of the fluid is assumed to vary according to a linearized equation of state

$$\rho_l = \rho_0\{1 - \alpha^*[T - T_L(C_0)] + \beta^*[C - C_0]\}, \tag{2.9a}$$

where α^* and β^* are constants. Within the mushy layer, this relationship can be written as

$$\rho_l = \rho_0[1 + \beta(C - C_0)], \tag{2.9b}$$

where $\beta = \beta^* - \alpha^* \Gamma$, by taking the liquidus relationship (2.6) into account. Note that β is usually positive since $\beta^*/\alpha^* \Gamma$ is typically much larger than unity. The combining in this way of the effects of temperature and composition on the density is valid once the strong coupling expressed by (2.6) is accepted. Note that this denies the possibility of any form of double-diffusive convection within the mushy region, which distinguishes the situations considered here from the convection in a porous medium below a fluid layer studied by Chen & Chen (1988).

Equations (2.1)–(2.9) constitute a full set of governing equations for the mushy layer. Two interfacial conditions that express conservation of heat and solute at both solid–mush and mush–liquid interfaces can be derived directly from equations (2.1). These can be expressed as

$$\mathscr{L}_s[\phi] V_n = [k_m \boldsymbol{n} \cdot \nabla T], \tag{2.10a}$$

$$(C - C_s)[\phi] V_n = [D_m \boldsymbol{n} \cdot \nabla C], \tag{2.10b}$$

where V_n is the normal velocity of the solid–mush or mush–liquid interface, $\boldsymbol{n}$ is a unit vector normal to the interface and [ ] denotes the jump in the enclosed quantity across the interface.

Worster (1986) introduced an additional condition to be applied at advancing mush–liquid interfaces. This condition is required in order to determine the unknown solid fraction ϕ. Worster argued that a solidifying system incorporating a mushy layer adopts a configuration of marginal thermodynamic equilibrium, which is achieved if the temperature gradient is equal to the gradient of the local liquidus temperature on the liquid side of the mush–liquid interface. This is expressed by

$$\boldsymbol{n} \cdot \nabla T = \Gamma \boldsymbol{n} \cdot \nabla C. \tag{2.11}$$

In addition to the thermodynamic interface conditions (2.10) and (2.11), we require that the pressure and the normal component of mass flux be continuous everywhere. Further boundary conditions will be introduced and discussed in the following sections in which specific examples are analysed.

3. A model of constrained growth

A convenient system to investigate mathematically is one that is steady in a frame moving with some prescribed, constant speed V, as illustrated in figure 2(*b*). The liquid region has fixed temperature T_∞ and composition C_0 as $z \to \infty$, where z measures vertical displacement in the moving frame. The temperature decreases downwards, and we consider cases in which a mushy zone separates a completely solid region from a completely liquid region. In this model problem we imagine that the eutectic front, at which the temperature is equal to the eutectic temperature T_e and below which the system is completely solid, can be maintained at the fixed horizontal position $z = 0$. The mush–liquid interface $z = h$ is left as a free boundary to be determined as part of the solution. In general $h = h(x, y)$ though, in the cases we shall consider, h is independent of the horizontal coordinates x and y.

We make the further simplification that all physical properties are constant and independent of phase. Then equations (2.1) can be written in the dimensionless form

$$-\frac{\partial \theta}{\partial z} + \boldsymbol{U} \cdot \nabla \theta = \nabla^2 \theta - \mathscr{S} \frac{\partial \phi}{\partial z}, \tag{3.1a}$$

$$\frac{\partial}{\partial z}[(1-\phi)(\mathscr{C} - \Theta)] + \boldsymbol{U} \cdot \nabla \Theta = \frac{1}{Le} \nabla \cdot [(1-\phi) \nabla \Theta] \tag{3.1b}$$

by scaling the fluid velocity with V and all lengths with the diffusive lengthscale $L = \kappa/V$, where $\kappa = k/c$ is the thermal diffusivity. The dimensionless temperature θ and concentration Θ are defined by

$$\theta = \frac{T - T_L(C_0)}{\Delta T}, \quad \Theta = \frac{C - C_0}{\Delta C}, \tag{3.2}$$

where $\Delta T = \Gamma \Delta C = T_L(C_0) - T_e$. Equations (3.1) apply throughout the region $z > 0$. The liquidus relationship

$$\theta = \Theta \tag{3.3}$$

applies within the mushy layer, while, in the liquid region, the temperature and composition are uncoupled and $\phi = 0$. The dimensionless parameters appearing in (3.1) are the Lewis number $Le = \kappa/D$, a Stefan number

$$\mathscr{S} = \frac{\mathscr{L}}{c\Delta T}, \tag{3.4}$$

and a concentration ratio

$$\mathscr{C} = \frac{C_s - C_0}{\Delta C} \tag{3.5}$$

that represents the compositional contrast between solid and liquid phases compared to the typical variations of concentration within the liquid. We shall see that $\mathscr{C}$ is an important parameter in determining the structure of the mushy layer.

Boundary conditions on the system of equations (3.1) are

$$\theta = -1 \quad (z = 0), \tag{3.6a}$$

$$\theta \to \theta_\infty, \quad \text{and} \quad \Theta \to 0 \quad (z \to \infty), \tag{3.6b}$$

where $\theta_\infty = (T_\infty - T_L(C_0))/\Delta T$. The interfacial conditions (2.10) and (2.11) applied at $z = h$ can be written

$$\mathscr{S}\phi = \left.\frac{\partial \theta}{\partial z}\right|_m - \left.\frac{\partial \theta}{\partial z}\right|_l, \tag{3.7a}$$

$$(\mathscr{C} - \Theta)\,\phi = \frac{1}{Le}\left(\left.\frac{\partial \Theta}{\partial z}\right|_l - (1-\phi)\left.\frac{\partial \Theta}{\partial z}\right|_m\right), \tag{3.7b}$$

$$\left.\frac{\partial \theta}{\partial z}\right|_l = \left.\frac{\partial \Theta}{\partial z}\right|_l. \tag{3.7c}$$

It is interesting to note that, in the absence of convection, the heat flux that needs to be extracted at $z = 0$ in order to maintain the steady state can be determined from (3.1*a*) by integrating the whole equation from $z = 0-$ to $z = \infty$ and using the boundary conditions (3.6). This procedure gives $\partial\theta/\partial z|_{0-} = 1 + \theta_\infty + \mathscr{S}$.

Hills *et al.* (1983) and Fowler (1985) have found complete analytical solutions that depend only upon z, for cases in which the fluid flow U is zero. These are repeated here in order to provide a basis for comparison with the convecting solutions derived in later sections of this paper. The temperature and concentration fields in the liquid region have the exponential forms

$$\theta = \theta_\infty + (\theta_i - \theta_\infty)\,e^{-(z-h)}, \tag{3.8}$$

$$\Theta = \theta_i\, e^{-Le(z-h)}, \tag{3.9}$$

where the dimensionless interfacial temperature is found, by applying (3.7*c*), to be

$$\theta_i = -\left(\frac{\theta_\infty}{Le-1}\right). \tag{3.10}$$

Within the mushy layer we let $Le \to \infty$, which simplifies the analysis and is physically reasonable since typically $D \ll \kappa$. With this approximation, it is readily shown from (3.7) that the interfacial conditions at $z = h$ become

$$\phi = 0, \quad \theta = 0, \quad \text{and} \quad \left[\frac{\partial\theta}{\partial z}\right] = 0 \quad (z = h). \tag{3.11}$$

The governing equations (3.1) can then be integrated to yield

$$\phi = \frac{-\theta}{\mathscr{C}-\theta}, \tag{3.12}$$

with θ given implicitly by

$$z = \frac{\alpha-\mathscr{C}}{\alpha-\beta}\ln\left(\frac{\alpha+1}{\alpha-\theta}\right)+\frac{\mathscr{C}-\beta}{\alpha-\beta}\ln\left(\frac{\beta+1}{\beta-\theta}\right), \tag{3.13}$$

where

$$\alpha = A+B, \quad \beta = A-B, \quad A = \tfrac{1}{2}(\mathscr{C}+\theta_\infty+\mathscr{S}), \quad B^2 = A^2-\mathscr{C}\theta_\infty.$$

The depth of the mushy layer is given simply by setting $z = h$, $\theta = 0$ in (3.13). Similar expressions to (3.12) and (3.13) are given by Hills *et al.* (1983).

A better understanding of how the system depends upon the three dimensionless parameters $\mathscr{S}$, $\mathscr{C}$, and θ_∞ can be gained by considering some limiting cases of (3.13). Several cases can be put into the simple form

$$z = \ln\left(\frac{\gamma+1}{\gamma-\theta}\right), \tag{3.14}$$

which can be inverted to yield the exponential temperature (concentration) profile

$$\theta = -\frac{e^{-z}-e^{-h}}{1-e^{-h}}, \quad \text{where} \quad h = \ln\left(1+\frac{1}{\gamma}\right). \tag{3.15}$$

The single parameter γ is given by

$$\gamma = \theta_\infty \qquad (\mathscr{C} \to \infty \text{ or } \mathscr{S} = 0 \text{ or } \theta_\infty \to \infty), \tag{3.16}$$

$$\gamma = \mathscr{S} \qquad (\mathscr{S} \to \infty), \tag{3.17}$$

$$\gamma = \theta_\infty + \mathscr{S} \quad (\mathscr{C} = 0). \tag{3.18}$$

The absence of $\mathscr{C}$ from these expressions is indicative of the dominant influence of thermal balances in determining the depth of the mushy layer, as pointed out by Huppert & Worster (1985). In the limiting cases of (3.16) the principal thermal balance is between conduction of heat through the mushy layer and conduction of heat from the liquid region. In (3.17) the balance is between conduction through the mushy layer and the latent heat released during solidification, while in (3.18) all three contributions to the thermal budget are in balance.

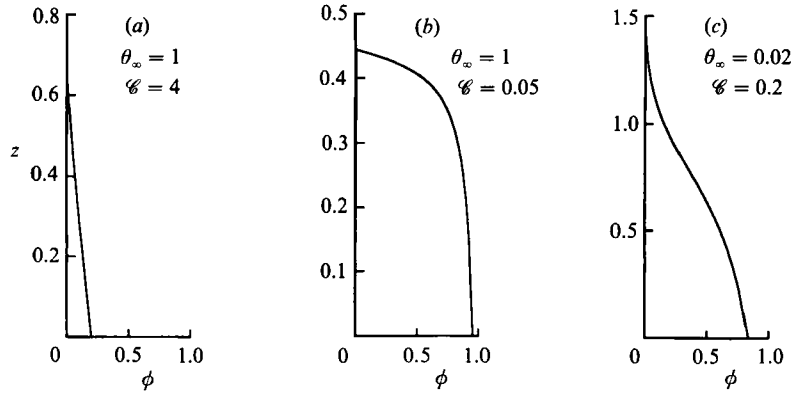

FIGURE 3. Various profiles of solid fraction ϕ as a function of height z in a mushy layer for different values of the concentration ratio $\mathscr{C}$ for $\mathscr{S} = 1$. (*a*) When $\mathscr{C}$ is large, the solid fraction is small throughout the layer. (*b*) When $\mathscr{C}$ is small, ϕ can be almost equal to unity through much of the layer. (*c*) For any value of $\mathscr{C}$, letting $\theta_0 \to 0$ produces a 'feathery' top to the layer, where the solid fraction is very small.

Another limiting case reveals one of the effects of varying $\mathscr{C}$. As $\theta_\infty \to 0$, so that heat transfer from the liquid region is weak, we obtain $\alpha \sim \mathscr{C} + \mathscr{S}$, $\beta \sim \mathscr{C}\theta_\infty/\alpha$ and

$$h \sim \frac{1}{\gamma}\ln\left(\frac{\gamma}{\theta_\infty}\right) \quad \text{with} \quad \gamma = \left(1 + \frac{\mathscr{S}}{\mathscr{C}}\right). \tag{3.19}$$

In this case, h does depend on $\mathscr{C}$ but only in a ratio with $\mathscr{S}$ in the single parameter γ. We see that increasing $\mathscr{C}$ is equivalent to decreasing $\mathscr{S}$ and thus that varying $\mathscr{C}$ acts to modify the amount of latent heat released.

In stagnant mushy layers, $\mathscr{C}$ affects the total solid fraction within the layer and thereby determines the necessary release of latent heat. Examples of how the solid fraction can vary with height are shown in figure 3. We see that $\mathscr{C}$ also affects the distribution of solid within the layer, as expressed by (3.12), and thus the mobility of the interstitial fluid and the nature of any flow that might take place.

When $\mathscr{C}$ is large, the solid fraction ϕ is small throughout the layer so the permeability is likely to be relatively uniform with depth. This situation, shown in figure 3(*a*), is typical of the experiments using aqueous solutions of ammonium chloride, for example. Conversely, figure 3(*b*) shows a case in which $\mathscr{C}$ is small, when the solid fraction is near unity in most of the layer. Here, the permeability is likely to be a strong function of depth and fluid flow may only penetrate the upper portions of the layer. These two pictures (figures 3*a* and 3*b*) represent the range of structures that can occur given moderate values of the other dimensionless parameters. Qualitatively different structures occur only when θ_∞ is very small. In such cases, as represented in figure 3(*c*), the function $\phi(z)$ has a point of inflexion, above which the solid fraction is very small. This behaviour is indicative of the loss of thermal control on the depth of the mushy layer that occurs when the heat flux from the liquid (proportional to θ_∞) tends to zero. When the heat flux is small, other physical effects not included in the present model, such as those related to surface energy or kinetic undercooling, become important and act to limit the growth of the layer.

In typical experiments with aqueous solutions of ammonium chloride, $\mathscr{C}$ is between about 10 and 20, and it is easy to arrange that θ_∞ is about unity. Thus, in what follows, we imagine that $\mathscr{C}$ is moderate or large and that θ_∞ is moderate so that

the structure of figure 3(*a*) pertains and the variation of the permeability of the layer with depth is small.

4. Natural convection

Dimensionless dynamical equations governing natural-convective flow in the system described in the previous section can be written as

$$\frac{1}{\sigma}\left(\frac{\partial \boldsymbol{u}}{\partial t}-\frac{\partial \boldsymbol{u}}{\partial z}+\boldsymbol{u}\cdot\nabla\boldsymbol{u}\right)=\nabla^2\boldsymbol{u}+R_T\theta\hat{\boldsymbol{z}}-R_C\left(\Theta\hat{\boldsymbol{z}}+\frac{\beta}{\beta^*}\nabla p\right) \tag{4.1}$$

in the liquid region and

$$\frac{\boldsymbol{U}}{\Pi}=-R_{\mathrm{m}}(\nabla p+\theta\hat{\boldsymbol{z}}) \tag{4.2}$$

in the mushy region, where Π is now scaled with Π_0, a typical dimensional value of the permeability of the mushy layer. At a mush–liquid interface, we require that

$$[p]=0 \quad \text{and} \quad [\boldsymbol{n}\cdot\nabla\boldsymbol{U}]=0, \tag{4.3}$$

where $\boldsymbol{n}$ is a unit vector normal to the interface.

These equations are coupled with the advection–diffusion equations (3.1) in both regions, subject to the boundary conditions (3.6) and interfacial conditions (3.11). Just as in §3, we let $Le\rightarrow\infty$ in the mushy region.

The fluid-dynamical behaviour of the crystallizing system is determined principally by the three Rayleigh numbers

$$R_T=\frac{\alpha^*\Delta T g L^3}{\kappa\nu}, \quad R_C=\frac{\beta^*\Delta C g L^3}{\kappa\nu}, \quad \text{and} \quad R_{\mathrm{m}}=\frac{\beta\Delta C g\Pi_0 L}{\kappa\nu}, \tag{4.4}$$

where ν is the kinematic viscosity of the fluid. The liquid region is characterized further by the Prandtl number $\sigma=\nu/\kappa$, the buoyancy ratio β/β^* and, since the temperature and concentration fields are uncoupled there, the Lewis number $Le=\kappa/D$. We note that it is often the case that $\beta^*/\alpha^*\Gamma\gg 1$, which implies that $R_T\ll R_C$ and $\beta/\beta^*\approx 1$.

Figure 4 shows the density fields due to temperature and composition of the static, steady state calculated in §3. Two extreme modes of buoyancy-driven convection can be envisaged.

One mode would arise if the permeability Π of the mushy layer were small. It is then possible that the fluid in the interstices remains almost stagnant while the liquid above it convects strongly. Since the thermal density variations are stabilizing while the compositional density variations are destabilizing, the possibility of double-diffusive, 'finger' convection can arise depending upon the relative magnitudes of R_T and R_C and on the value of Le (Turner 1979). This mode of convection would be characterized by having a critical wavelength comparable with the thickness of the compositional boundary layer.

Alternatively, since the change in concentration across the compositional boundary layer is typically small, of order $\theta_\infty Le^{-1}\ll 1$, compared to that across the mushy layer (see (3.9) and (3.10)) and the boundary layer is thin, of order Le^{-1}, compared to the depth of the mushy layer, it is possible that the compositional boundary layer is convectively stable while the mushy layer is convectively unstable. This second mode of convection would be characterized by having velocity fields of equal magnitude in the liquid and mushy regions and by having horizontal

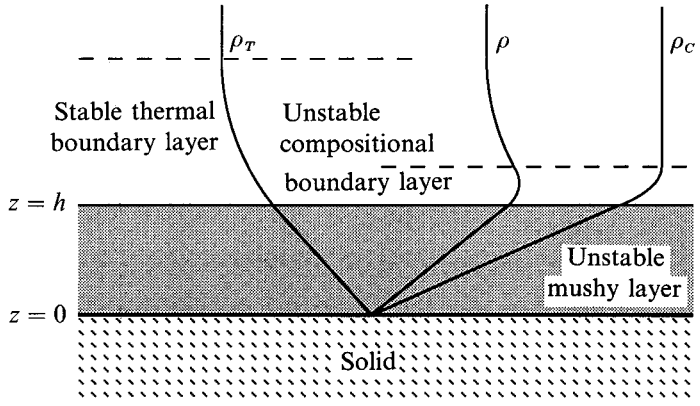

FIGURE 4. A schematic diagram showing the density variations due to temperature, ρ_T, and composition, ρ_C, and the total density field, ρ.

wavelengths comparable with the depth of the mushy layer. The flow in the liquid region, in this case, is driven solely in response to the convection arising from the mushy layer.

In order to determine whether either mode or both modes of convection occur, it is necessary to conduct a detailed stability analysis. However, for the first mode, in which the interstitial liquid in the mushy region is essentially stagnant, many previous results (Turner 1979) can be applied to estimate the tendency for convective instability of the liquid region. If the permeability of the mushy layer is very small then it acts almost as a solid boundary as far as the flow in the liquid region is concerned. The compositional boundary layer is unstable once a local Rayleigh number $R_{\delta C} = Le^{-3}R_C$, based upon the depth of the compositional boundary layer and on the solutal rather than the thermal diffusivity, exceeds a critical value of about 10 (Hurle, Jakeman & Wheeler 1983). However, we note that the ratio of the total destabilizing potential energy in the compositional boundary layer to the total stabilizing potential energy in the thermal boundary layer is of order $Le^{-2}(\beta^*/\alpha^*\Gamma)$, which can be small, since typically $Le \gg 1$, even though the buoyancy ratio $\beta^*/\alpha^*\Gamma$ is usually large. Thus, in this case, 'finger' convection in a small region above the mushy layer is perhaps more likely than the wholescale disruption of the thermal boundary layer found by Woods & Huppert (1989) above a plane solidification front. Indeed, such convection was observed in the experiments of Tait & Jaupart (1989) in which ammonium-chloride mushy layers were grown from aqueous solutions doped with hydroxyethylcellulose, which increased the viscosity of the liquid and suppressed convection of the interstitial fluid in the mushy layer.

We shall concentrate here on the convection of the interstitial fluid within the mushy layer and therefore consider the second mode of convection in which the liquid region is convectively stable. This can occur if the local compositional Rayleigh number $R_{\delta C}$ is sufficiently small. At the same time, we require that R_{m} is sufficiently large (Fowler 1985) for convection to occur in the mushy layer. These two conditions can be achieved simultaneously if $Le^3 \Pi_0 L^{-2} \gg 1$.

It is instructive to consider the make-up of R_{m}, which is the sole dimensionless parameter governing convection in the mushy layer. Like the other Rayleigh numbers, it is the ratio of the destabilizing potential energy available to a disturbed fluid element to the stabilizing dissipation of that energy as the element moves. In this case, the Rayleigh number depends upon the destabilizing influence of

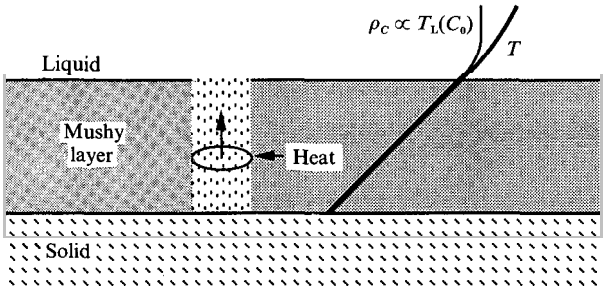

FIGURE 5. A schematic diagram illustrating the convective instability of a parcel of fluid within a mushy layer and the formation of a chimney. The temperature T and the density due to the solute concentration ρ_C both increase with height. The fluid parcel is considered to be much larger than the spacing between dendrites.

compositional buoyancy but on the stabilizing influence of *thermal* diffusion. To understand the physical reasons for this, consider the schematic diagram of figure 5. When a fluid element is displaced slightly upwards, it finds itself buoyant relative to its surroundings since the fluid density of the surroundings increases upwards owing to compositional variations. However, the fluid element also finds itself cooler than its surroundings. It therefore warms up by thermal diffusion but, owing to the much slower diffusion of solute, does not change its concentration appreciably. This much would be true in a passive porous medium and could lead either to ordinary buoyancy-driven convection or to the double-diffusive phenomenon of 'salt fingers' (Turner 1979; Chen & Chen 1988). In the reactive mushy layer, however, the raised fluid element, which has a temperature close to its new environment but is relatively depleted of solute, partly dissolves the dendrites that it encompasses. It thereby becomes denser and dissipates its potential energy. Thus the physical balance expressed in R_m is that between compositional buoyancy and the dissipation of that buoyancy arising from exchanges of solute between the liquid and solid phases caused by thermal diffusion. Such behaviour is analogous to aspects of 'wet convection', studied in relation to cloud physics, in which parcels of moist air can change their density through evaporation or condensation as well as through thermal expansion.

Note that the parcel argument just outlined relies upon two fundamental assumptions of our modelling: that the spacing between dendrites is smaller than the lengthscale of typical fluid motions, so that the fluid element encompasses several dendrites; and that the mushy layer can be maintained near equilibrium, through internal melting or solidification, on a timescale that is short compared with the transport times of fluid motions.

Another feature emerges from this parcel argument, namely that where fluid rises, dendrites melt and hence the permeability increases. It may be possible that a rising plume can completely dissolve the dendrites that it encompasses to form a 'chimney' in the mushy layer. This has been observed in experiments and we shall now formalize this picture using the mathematical model presented in §§2 and 3.

5. The structure of a convecting mushy layer

The dimensionless governing equations presented in §§3 and 4 can be used to determine a critical value of the Rayleigh number R_m above which a stagnant mushy layer is convectively unstable to infinitesimal disturbances (Fowler 1985). Here, we

aim rather to find strongly nonlinear solutions that describe the convective flow in a mushy layer once chimneys are fully developed. Specifically, we seek steady solutions under the assumption that R_m is large.

This section begins with the derivation of asymptotic equations governing the regions of the mushy layer that are outside the immediate vicinity of chimneys. It is then argued that rapid upflow occurs in narrow, vertical regions and causes chimneys to form. Flow in the chimneys is governed by the Navier–Stokes equations. The major part of the section is devoted to a scaling analysis of the thermal boundary layer that surrounds each chimney in order to demonstrate that, to leading order, the pressure driving the flow in the chimneys is given simply by the hydrostatic pressure in the outer regions of the mushy layer. Thus an important, simplifying feature of the analysis is that, when R_m is large, the flow in the outer regions of the mushy layer is independent of the functional form of the relationship between porosity and permeability (2.8). An explicit form of this equation is needed to determine the detailed structure of the boundary layer and the overall number density of chimneys, neither of which is addressed in this paper.

Formally, we let $R_m \to \infty$ and look for solutions in which $|\boldsymbol{U}|$ remains of order unity. This can be achieved consistently provided that the dimensionless number density of chimneys $\mathcal{N}$ (equal to the number of chimneys per unit horizontal area multiplied by L^2) is not too large. The specific upper bound $\mathcal{N}_{\max}$ on the allowed magnitude of $\mathcal{N}$ is found towards the end of this section. While there is no external control over the value of $\mathcal{N}$ and it is perhaps to be expected that $|\boldsymbol{U}| \to \infty$ as $R_m \to \infty$, it is possible to find solutions to the governing equations with $|\boldsymbol{U}| = O(1)$ for any prescribed value of $\mathcal{N}$ with $0 \leqslant \mathcal{N} < \mathcal{N}_{\max}$. The question that must be asked is whether any of these solutions are stable. A discussion of this question is presented in §7.

Equation (4.2) shows that, to leading order in large R_m, while $|\boldsymbol{U}| = O(1)$, the pressure field is hydrostatic and θ is independent of horizontal position. Equations (3.1*a*, *b*) then show, in this limit, that ϕ and the vertical component W of the velocity are also functions of z only.

The governing equations for the leading-order variables $\theta_0(z)$, $\phi_0(z)$ and $W_0(z)$ when $R_m \gg 1$ are thus

$$(W_0 - 1)\,\theta_0' = \theta_0'' - \mathscr{S}\phi_0', \tag{5.1a}$$

$$(1-\phi_0)\,\theta_0' + \mathscr{C}\phi_0' = W_0\,\theta_0', \tag{5.1b}$$

where primes denote differentiation with respect to z. These equations are derived from (3.1) with $Le^{-1} = 0$.

When $W_0 = 0$, as in §3, the two terms on the left-hand side of (5.1*b*) must balance, and hence large values of $\mathscr{C}$ lead to small values of the solid fraction ϕ_0, as illustrated in figure 3(*a*). However, when W_0 is non-zero, and $\mathscr{C}$ is large, the second term on the left-hand side can dominate the first term and balance the advective term on the right-hand side. When this occurs, it is readily seen from (5.1*b*) that W_0 is negative (i.e. the flow is downwards) everywhere to leading order. However, in order to satisfy global mass conservation, there must be upwards flow somewhere. The scaling arguments proposed here therefore indicate that, when R_m is large, the upflow can only occur in regions that are narrow compared with the scale-depth $L = \kappa/V$ and, by continuity, the upwards flow in these regions must be correspondingly large.

It was argued in §4 that upflow causes the solid fraction of the mushy layer to decrease locally. Further, Fowler (1985) has suggested that the solid fraction becomes zero once the dimensionless upflow exceeds unity. Thus, given the proposed scalings, a possible structure for the convecting mushy layer is that illustrated in

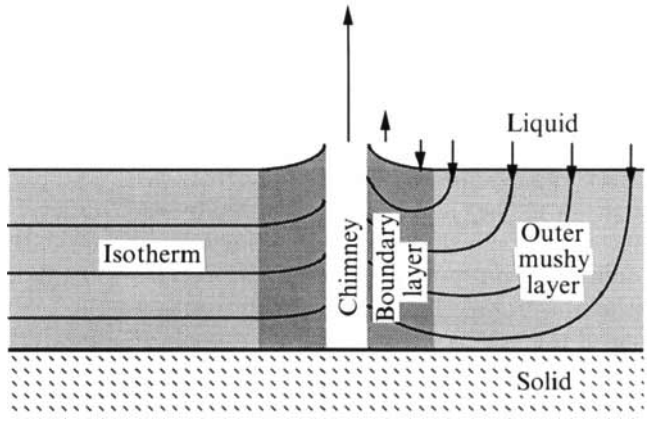

FIGURE 6. A schematic diagram representing the structure of a convecting mushy layer once steady convection through chimneys is fully developed. Isotherms in the mushy layer are shown to the left of the chimney while the vertical component of velocity (arrows) and streamlines are shown to the right. There is inflow to the chimney at all heights. In the boundary layer, the temperature decreases, the vertical velocity changes sign and the solid fraction increases towards the chimney.

figure 6. Throughout most of the layer, the solid fraction is horizontally uniform and the vertical component of the flow is downwards. The layer is interspersed with chimneys of zero solid fraction in which the vertical component of the flow is upwards. Around each chimney there is a thermal boundary layer that forms as the mushy layer is cooled locally by the fluid rising through the chimney. This picture is consistent with experimental observations in aqueous, ammonium-chloride systems (Copley *et al.* 1970) and in some metallic systems (Sarazin & Hellawell 1988).

In order to determine the downwards flow $W_0(z)$ in the 'outer' regions of the mushy layer (away from chimneys), and hence to complete the description provided by (5.1), it is necessary to analyse the flow in the chimneys and surrounding boundary layers. A chimney is characterized by being devoid of dendrites, so the flow in a chimney must be described by the Navier–Stokes equations. Dimensionless equations describing the temperature, concentration and velocity fields within a chimney can be approximated by

$$-\frac{\partial\theta}{\partial z}+\boldsymbol{u}\cdot\boldsymbol{\nabla}\theta=\nabla^2\theta, \tag{5.2a}$$

$$-\frac{\partial\Theta}{\partial z}+\boldsymbol{u}\cdot\boldsymbol{\nabla}\Theta=0, \tag{5.2b}$$

$$\nabla^2\boldsymbol{u}=R_C(\Theta\hat{\boldsymbol{z}}+\boldsymbol{\nabla}p), \tag{5.2c}$$

$$\boldsymbol{\nabla}\cdot\boldsymbol{u}=0. \tag{5.2d}$$

These equations are obtained from (2.1), (2.5) and (4.1) by letting $Le\to\infty$, $\beta=\beta^*$, $R_T=0$ and $\sigma\to\infty$. The first three of these approximations have been discussed and justified previously, while letting $\sigma\to\infty$ is a simplifying assumption that we make here for convenience but which is appropriate for many liquids.

If we assume further that the chimney is axisymmetric then the continuity equation (5.2*d*) can be satisfied by introducing a Stokes stream function ψ such that

$$\boldsymbol{u}=\left(-\frac{1}{r}\frac{\partial\psi}{\partial z},\frac{1}{r}\frac{\partial\psi}{\partial r}\right) \tag{5.3}$$

with respect to local radial and axial coordinates (r, z).

If the radius of a chimney $a(z) = O(\epsilon)$, where $\epsilon \ll 1$ when $R_m \gg 1$, $R_C \gg 1$, then consistent scalings for the dependent variables within the chimney are as follows. The stream function $\psi = O(\epsilon^4 R_C)$, the composition $\Theta = O(1)$ and, if the temperature field is written in the form

$$\theta \sim \theta_0(z) + \theta_1(r, z), \tag{5.4}$$

then the deviation from the outer solution $\theta_1 = O(\epsilon^4 R_C)$. We shall see that $\epsilon^4 R_C \ll 1$ while the magnitude of the vertical velocity within the chimney $\epsilon^2 R_C \gg 1$. With these scalings, the leading-order governing equations for the chimney are

$$\frac{1}{r}\frac{\partial}{\partial r}\left(r\frac{\partial \theta_1}{\partial r}\right) = \theta_0' \frac{1}{r}\frac{\partial \psi}{\partial r}, \tag{5.5a}$$

$$\boldsymbol{u}\cdot\nabla\Theta = 0, \tag{5.5b}$$

$$\frac{1}{r}\frac{\partial}{\partial r}\left(r\frac{\partial w}{\partial r}\right) = R_C(\Theta - \theta_0), \tag{5.5c}$$

with corrections of $O(\epsilon^2 R_C)^{-1}$. In (5.5*c*) we have used the fact that, to leading order, the pressure everywhere is equal to the hydrostatic pressure in the outer regions of the mushy layer, which will be demonstrated shortly.

The diameter of a chimney is determined by thermal balances in the boundary layer surrounding it. The heat flux from the cold, rising fluid in a chimney, determined by integrating (5.5*a*), is

$$2\pi a \left.\frac{\partial \theta_1}{\partial r}\right|_{r=a} = 2\pi \psi_a \theta_0', \tag{5.6}$$

where $2\pi\psi_a$ is the vertical volume flux in the chimney. These fluxes must be balanced by the diffusion of heat and a flow of interstitial fluid from the mushy layer into the chimney. Hence, as $r \to a$ through the boundary layer,

$$\theta - \theta_0 = \theta_1 \sim \psi_a \theta_0' \ln r, \tag{5.7}$$

$$U \sim -\psi_a' \frac{1}{r}. \tag{5.8}$$

The horizontal flow U is driven by a horizontal pressure gradient across the boundary layer that is given by (4.2). The permeability remains of order unity in the boundary layer since the temperature variations within it, given by (5.7) are small, as we shall see. Thus the pressure near the chimney has magnitude

$$\Delta p \sim \frac{\psi_a'}{R_m} \ln \epsilon \tag{5.9}$$

with respect to the hydrostatic pressure in the outer regions of the mushy layer. Finally, the perturbation in the concentration field, represented by (5.7), drives an upward flow of magnitude

$$W \sim R_m \psi_a \ln \epsilon \tag{5.10}$$

near the wall of the chimney, since both Π and θ_0' are of order unity.

Now, as r decreases from the outer edge of the boundary layer towards the edge of the chimney, the solid fraction ϕ first increases because of the additional cooling and then decreases as the flow turns upwards bringing with it depleted fluid that

dissolves the dendrites. This requires a balance of all the terms in (3.1*b*) throughout the boundary layer, which leads to two possible scalings depending upon the relative magnitudes of R_C and R_m.

When R_C is relatively small compared to R_m, it can be shown (Appendix A) that the vertical flow W in the boundary layer near the wall of the chimney is $O(1)$ and that the vertical advection of solute exceeds the horizontal advection. This gives the scalings

$$\epsilon^4 \ln \epsilon \sim (R_m R_C)^{-1}, \tag{5.11a}$$

$$\Delta p \sim R_m^{-2}, \tag{5.11b}$$

$$\theta - \theta_0 \sim R_m^{-1}. \tag{5.11c}$$

These scalings become invalid once $R_C \sim (R_m \ln \epsilon)^3$, with ϵ given by (5.11*a*). At this point, the horizontal advection of solute becomes of equal magnitude with the vertical advection. Once $R_C \gg (R_m \ln \epsilon)^3$ the following scalings are appropriate (Appendix A):

$$\frac{\epsilon^2}{\ln \epsilon} \sim \frac{R_m}{R_C}, \tag{5.12a}$$

$$\Delta p \sim (\epsilon \ln \epsilon)^2 \sim R_m^{-2} \frac{(R_m \ln \epsilon)^3}{R_C}, \tag{5.12b}$$

$$\theta - \theta_0 \sim R_m^{-1} \left[\frac{(R_m \ln \epsilon)^3}{R_C} \right]^{\frac{1}{2}}. \tag{5.12c}$$

Vertical and horizontal advection of solute balance throughout this regime and (3.1*b*) shows additionally that $\partial \phi / \partial z \sim (R_m \epsilon \ln \epsilon)^2 \ll 1$, which in turn shows that $a'(z)/a \ll 1$, i.e. that the wall of the chimney is vertical to leading order.

Both sets of scalings (5.11) and (5.12) have the properties that $\Delta p \ll 1$ and $\theta - \theta_0 \ll 1$ when $R_m \gg 1$. This justifies our approximation of using the hydrostatic pressure in (5.5*c*) and our earlier statement that Π remains of order unity. We shall continue with the second set of scalings (5.12) principally because it leads to the simplifying feature that the chimney radius a is constant with height.

We note that the radii of chimneys are observed experimentally to be approximately constant with height in mushy layers that form above a solid, eutectic layer, though the radius tends to increase rapidly near the base of mushy layers that form above a cooled surface whose temperature is maintained greater than the eutectic temperature.

The alternative set of scalings (5.11) will not lead to qualitatively different results for the global structure of the mushy layer but is quantitatively more difficult to work with. We also focus on determining the total fluxes of fluid, solute and heat rather than the detailed characteristics of the field variables within chimneys and their surrounding boundary layers.

The volume flux through a chimney can be estimated by applying integral constraints derived from (5.5) to suitable trial functions for the concentration and velocity fields (Roberts & Loper 1983; and Appendix B of this paper). The total volume flux is given by

$$2\pi \psi_a = 2\pi \lambda a^4 R_C (1 + \theta_0(z)), \tag{5.13}$$

where $\lambda \approx 0.0306$, as shown in Appendix B. In order to satisfy global mass conservation, the downflow through the bulk of the mushy layer $W_0(z)$ must equal the total upflow through all the chimneys per unit horizontal area. Thus

$$W_0(z) = -2\pi \psi_a \mathcal{N}, \tag{5.14}$$

where $\mathcal{N}$ is the dimensionless number density of chimneys. If we define

$$\mathcal{F} = 2\pi\lambda a^4 R_C \mathcal{N}, \tag{5.15}$$

which is a constant, independent of z, then

$$W_0(z) = -\mathcal{F}(1+\theta_0(z)). \tag{5.16}$$

The foregoing scaling analysis was founded on the assumption that $\mathcal{N}$ is not too large, so that $W_0 = O(1)$. We see now that this requires specifically that

$$\mathcal{N} < [\epsilon^4 R_C]^{-1} \sim R_m \ln\epsilon, \tag{5.17a}$$

for the first scaling (5.11), or

$$\mathcal{N} < [\epsilon^4 R_C]^{-1} \sim R_m \ln\epsilon \left[\frac{R_C}{(R_m \ln\epsilon)^3}\right], \tag{5.17b}$$

for the second scaling (5.12). Since the right-hand sides of (5.17) are much larger than unity when $R_m \gg 1$, these conditions are not very restrictive.

What has been achieved is an expression for the vertical flow in the outer regions of the mushy layer (5.16) in terms of the single parameter $\mathcal{F}$. This parameter is determined partly by the dynamics local to each chimney, which determines a, and partly by the global dynamics of the mushy layer that determine $\mathcal{N}$. It is useful to recognize $\mathcal{F}$ as the ratio of the convective velocity from the overlying melt into the mushy layer to the rate of solidification V.

We note finally that the dimensional fluxes of solvent F_C and of heat F_T convected from the mushy layer into the overlying liquid region are

$$F_C = -\tfrac{1}{2}\mathcal{F} V(C_0 - C_b) \tag{5.18}$$

and

$$F_T = -\mathcal{F} V(T_\infty - T_L(C_0)). \tag{5.19}$$

Equation (5.18) is obtained by integrating (5.5b) across a horizontal cross-section of a chimney, while (5.19) is obtained by noting that, to leading order, the temperature of the liquid in the chimney is horizontally uniform and equal to the temperature in the surrounding mushy layer.

6. The effects of convection

The simple relationship (5.16) for the fluid flow as a function of the solute field in the bulk of the mushy layer can be incorporated into (5.1) to determine the gross effects of convection on the mushy layer. If we assume that the motion of the overlying fluid is driven by continuity of mass, solely in response to the motions in the mushy layer, then we can integrate equation (3.1a) with $\phi = 0$ to find the temperature field there,

$$\theta = \theta_\infty \left[1 - e^{-(1+\mathcal{F})(z-h)}\right]. \tag{6.1}$$

By using (6.1) to determine the boundary conditions (3.11), equations (5.1) can each be integrated once to give

$$\theta_0' = -\theta_0 + \mathcal{S}\phi_0 + \theta_\infty(1+\mathcal{F}) + \tfrac{1}{2}\mathcal{F}[1-(1+\theta_0)^2] \tag{6.2}$$

and

$$(1-\phi_0)(\mathcal{C}-\theta_0) = \mathcal{C} - \tfrac{1}{2}\mathcal{F}[1-(1+\theta_0)^2]. \tag{6.3}$$

Equation (6.3) gives ϕ_0 as a function of θ_0, and the remaining first-order differential equation (6.2) is readily integrated numerically to determine θ_0. Some results are

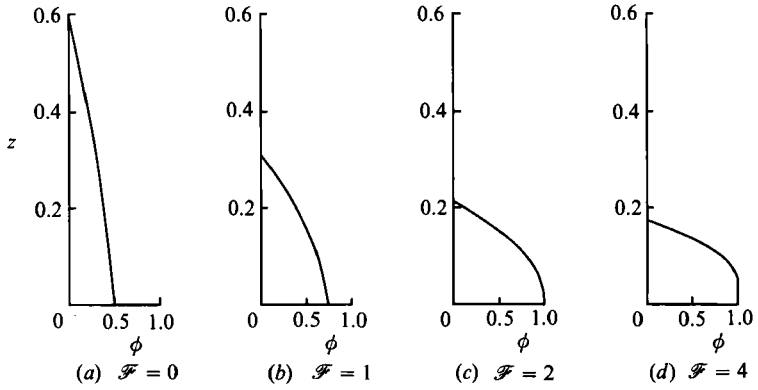

FIGURE 7. Computed profiles of solid fraction ϕ as a function of height z for various values of the parameter $\mathscr{P}$. Increasing values of $\mathscr{P}$ correspond to increasing values of the number density of chimneys and hence to increasing vigour of the convective flow.

displayed in figure 7 to show the effects of increasing $\mathscr{P}$ while the other dimensionless parameters are held constant and equal to unity. The figure shows the solid fraction as a function of height for several different values of $\mathscr{P}$. Two very important features are illustrated. First, as the strength of convection increases (signified by increasing $\mathscr{P}$) the depth of the mushy layer decreases. This is a direct result of the additional heat that is convected from the overlying liquid region which tends to inhibit growth of the mushy layer. Secondly, convection carries more solute from the overlying liquid into the mushy layer, which allows further internal solidification and an increase in the solid fraction. Indeed, one sees, by applying the boundary condition (3.6a) to (6.3), that the liquid fraction at the base of the mushy layer,

$$1-\phi_0(0) = \frac{\mathscr{C}-\frac{1}{2}\mathscr{P}}{1+\mathscr{C}}, \tag{6.4}$$

decreases linearly with $\mathscr{P}$ until it is zero when $\mathscr{P} = 2\mathscr{C}$. This gives us the maximum allowed value of $\mathscr{P}$ for the validity of the present model.

For greater values of $\mathscr{P}$, the liquid fraction tends to zero as $z \to z_c > 0$ from above. If we redefine the base of the mushy layer to be at $z = z_c$ and assume (see the discussion in §7) that the structure found in §5 remains valid in $z > z_c$, where the liquid fraction is still of order unity, then equation (5.16) for the vertical velocity becomes

$$W_0(z) = -\mathscr{P}[\theta_0(z)-\theta_c], \tag{6.5}$$

where $\theta_c = \theta_0(z_c)$. Equations (6.2) and (6.3) are then replaced by

$$\theta_0' = -\theta_0 + \mathscr{S}\phi_0 + \theta_\infty(1-\mathscr{P}\theta_c) + \tfrac{1}{2}\mathscr{P}[\theta_c^2-(\theta_0-\theta_c)^2] \tag{6.6}$$

and

$$(1-\phi_0)(\mathscr{C}-\theta_0) = \mathscr{C}-\tfrac{1}{2}\mathscr{P}[\theta_c^2-(\theta_0-\theta_c)^2]. \tag{6.7}$$

Since $\phi_0 = 1$ at $z = z_c$, where $\theta_0 = \theta_c$, equations (6.6) and (6.7) imply that

$$\theta_c = -\left(\frac{2\mathscr{C}}{\mathscr{P}}\right)^{\frac{1}{2}} \tag{6.8a}$$

and

$$\theta_c' = -\theta_c + \mathscr{S} + \theta_\infty(1-\mathscr{P}\theta_c) + \mathscr{C}. \tag{6.8b}$$

These values of θ and its derivative at $z = z_c$ must match with the completely solid region below $z = z_c$. In the solid region, θ obeys a simple diffusion equation, whose solution is

$$\theta = -1 + A(1 - e^{-z}), \tag{6.9}$$

where A is a constant, from which it can be determined that

$$z_c = \ln\left(1 + \frac{1+\theta_c}{\theta_c'}\right), \tag{6.10}$$

with θ_c and θ_c' given by (6.8). This result, together with (6.6) and (6.7) were used to plot the case $\mathscr{F} = 4$ in figure 7(*d*).

7. Discussion

An analysis of the governing equations for a mushy layer has produced mathematical solutions that incorporate the effects of strong natural convection. The results are formally valid in the asymptotic regime $R_m \gg 1$ provided that the dimensionless number density of chimneys $\mathscr{N}$ is less than order $(\epsilon^4 R_C)^{-1}$, with ϵ given by $\epsilon \ln \epsilon = (R_m R_C)^{-1}$ if $R_C \ll R_m^3$ or by $\epsilon^2/\ln \epsilon = R_m/R_C$ if $R_C \gg R_m^3$. Here, R_m is a Rayleigh number for the mushy layer and R_C is a solutal Rayleigh number for the liquid. These solutions provide some evidence of the suitability of the governing equations for describing mushy layers that are observed experimentally.

From a qualitative point of view, the solutions presented in this paper demonstrate that the observed structure of some convecting mushy layers (such as those produced from aqueous solutions of ammonium chloride, for example), having convection through narrow chimneys interspersed through the layer, is consistent with the proposed governing equations. The width of the chimneys predicted by the theory were shown to be of order $\epsilon \ll 1$, compared with the depth of the layer, when $R_m \gg 1$. The pressure field was shown to be almost hydrostatic (i.e. that $\nabla p = \rho \boldsymbol{g}$ throughout the layer), and this approximation led to a simple expression for the vertical component of the velocity field in terms of the local concentration of the interstitial fluid.

An interesting result that emerges from the scaling analysis is that the volume flux through an individual chimney decreases as the Rayleigh number R_m increases. This is just one of the curious ways in which convection in a mushy layer differs from that in a passive porous medium. In vertical convection boundary layers there is always a competition between the increasing mean vertical velocity and the narrowing of the boundary layer as the Rayleigh number increases. In a Newtonian fluid, or in a passive porous medium, the net effect of these two processes is to increase the vertical volume flux in the boundary layer. In the mushy layer there is an additional, thermodynamical element in the competition which acts to enhance freezing and to diminish the width of the boundary layer (chimney) further as the Rayleigh number increases. The net effect in this case is to decrease the vertical volume flux through a chimney. It is to be expected, perhaps, that the number density of chimneys that occurs in practice will increase with the Rayleigh number in such a way as to increase the total volume flux of fluid exchanged between the mushy layer and the overlying liquid region. However, such a prediction is outside the scope of the present theory.

The expression for the vertical component of velocity in the mushy layer in terms of the local solute field allowed a family of solutions to be found for the leading-order

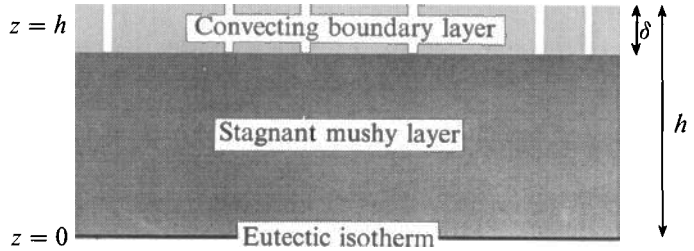

FIGURE 8. A schematic diagram showing the structure of the mushy layer when R_m is extremely large so that $\mathscr{F} > 2\mathscr{C}$. Most of the layer is stagnant, having very small, or zero, permeability. There is a boundary layer at the top of the mushy layer in which the porosity χ is of order unity and through which vigorous convection occurs. The structure of this boundary layer is similar to the structure of the whole mushy layer depicted in figure 6 with vertical flow through chimneys dispersed throughout the layer.

structure of the mushy layer away from chimneys, characterized by a single parameter $\mathscr{F}$ that is linearly related to the number density of chimneys $\mathscr{N}$ and is equal to the ratio of the convective fluid velocity at the mush–liquid interface to the rate of solidification. As $\mathscr{F}$ increases, the convective exchange of fluid between the mushy layer and the overlying liquid region increases. This was shown to cause the depth of the mushy layer to decrease and the solid fraction to increase. These are both stabilizing effects causing the local Rayleigh number, based upon the depth of the mushy layer and the compositional contrast across it, to decrease.

The solutions found are self-consistent solutions of the governing equations provided that $\mathscr{F} < 2\mathscr{C}$. This gives a definition for $\mathscr{N}_{\max} = O(\epsilon^{-4} R_C^{-1} \mathscr{C})$, the maximum allowed value of $\mathscr{N}$ for the theory to be valid. It is natural to ask whether any of these solutions are stable and whether, therefore, they correspond to experimentally observable states. Specifically, given a large, prescribed value of R_m one can ask whether there is a value of $\mathscr{N}$, $\mathscr{N}_c < \mathscr{N}_{\max}$, above which the solutions that have been found are stable.

There are two reasons for believing that the solutions can sometimes be stable for a value of $\mathscr{N} < \mathscr{N}_{\max}$. The first is that we have shown that $\mathscr{N}_{\max} \gg 1$ when $R_m \gg 1$ whereas experiments have tended to show that $\mathscr{N}$ is about unity in practice. The second is that the upper limit $\mathscr{F} = 2\mathscr{C}$ corresponds to solutions that have zero liquid fraction χ at $z = 0$. However, I have estimated that the liquid fraction, which decreases as $\mathscr{F}$ increases, is greater than about 0.6–0.7 throughout the mushy layer in my own experiments with ammonium chloride, and C. F. Chen (private communication) has measured the liquid fraction using X-ray tomography to be about 0.6 at $z = 0$ in his experiments with ammonium chloride.

The experiments with aqueous solutions of ammonium chloride are characterized by large values of $\mathscr{C}$, so it may be that these systems fall fortuitously into the category of operating with $\mathscr{F} < 2\mathscr{C}$. It is important to consider how a system will behave when either $\mathscr{C}$ is small or R_m is so large that $\mathscr{F}_c > 2\mathscr{C}$.

Both cases can be determined by considering the limit $R_m \to \infty$ while relaxing the condition $|U| = O(1)$ imposed in §5. The mushy layer then adopts the structure shown in figure 8, which is similar to that suggested by the solutions presented in figures 3(*c*) and 7(*d*). The depth of the mushy layer is determined by thermal balances and has magnitude $h \sim 1/|U|$. However, through most of its depth, the mushy layer has $\chi = 0$; the interstices are efficiently filled in by the extra solute transported by the vigorous convection. (It is possible that χ is greater than zero in

this region if the permeability tends to zero at some non-zero value of χ, which would lead to trapped liquid inclusions.) There is a narrow boundary layer of thickness δ near the mush–liquid interface in which χ increases to unity and the interstitial fluid convects. The temperature contrast across this boundary layer has magnitude $\Delta\theta \sim \delta/h$, derived by balancing thermal fluxes in the mushy layer. The balance of convective transport with generation of solvent within the mushy layer is expressed by $\boldsymbol{U}\cdot\boldsymbol{\nabla}\Theta \sim \mathscr{C}\,\partial\phi/\partial z$, which gives $|\boldsymbol{U}|\Delta\theta \sim \mathscr{C}$.

The magnitude of $|\boldsymbol{U}|$ is still indeterminate. However, if $\mathscr{F}(\mathscr{N})$ increases until the system regains stability then we can conjecture that the local Rayleigh number $R_\delta = R_m\,\delta\Delta\Theta$, based upon the thickness δ of the boundary layer and the compositional contrast $\Delta\Theta = \Delta\theta$ across it, remains of order unity as $R_m \to \infty$. This hypothesis is introduced by analogy with the convective state that occurs when a deep fluid layer is heated from below (Howard 1966). The scalings presented in the previous paragraph together with this hypothesis lead to

$$|\boldsymbol{U}| \sim \mathscr{C}^{\frac{2}{3}}R_m^{\frac{1}{3}}, \quad h \sim \mathscr{C}^{-\frac{2}{3}}R_m^{-\frac{1}{3}}, \quad \delta \sim \mathscr{C}^{-\frac{1}{3}}R_m^{-\frac{2}{3}}, \quad \Delta\theta \sim \mathscr{C}^{\frac{1}{3}}R_m^{-\frac{1}{3}}. \tag{7.1}$$

If we now rescale the variables by $\boldsymbol{U} = \mathscr{C}^{\frac{2}{3}}R_m^{\frac{1}{3}}\boldsymbol{U}^*$, $\theta = \mathscr{C}^{\frac{1}{3}}R_m^{-\frac{1}{3}}\theta^*$ etc. then Darcy's equation becomes

$$\frac{\boldsymbol{U}^*}{\Pi} = -R_m^*(\boldsymbol{\nabla}p + \theta^*\hat{\boldsymbol{z}}), \tag{7.2}$$

where $R_m^* = \mathscr{C}^{-\frac{1}{3}}R_m^{\frac{1}{3}}$, and $\delta/h = (R_m^*)^{-1}$. Therefore, if $R_m \gg 1$ then $R_m^* \gg 1$, the structure of figure 8 pertains and, since $|\boldsymbol{U}^*| = O(1)$, the scaling analysis of §5 can be applied within the upper boundary layer, which will thus have the structure depicted in figure 6.

Fearn, Loper & Roberts (1981) suggested that the Earth's inner core is a mushy zone of iron dendrites extending all the way to the Earth's centre. Loper (1983) later showed that the solid fraction increases rapidly with distance inwards from the inner-core boundary by constructing Taylor series of the dependent variables from the equations for a mushy layer proposed by Hills *et al.* (1983). Since the outer core is thought to consist of a molten mixture of iron and *small* amounts of other light components (e.g. oxygen and sulphur), the value of $\mathscr{C}$ appropriate to the freezing of the inner core is likely to be small. We should therefore anticipate that the picture in figure 8 is appropriate to describe the structure of the inner core; a picture that is consistent with the estimates of Loper (1983).

8. Conclusions

The essential physical processes governing convection through chimneys in a mushy layer have been elucidated by an asymptotic analysis of simplified governing equations. The important processes were found to be thermal balances, modified by free compositional convection, controlling the overall depth of the mushy layer and the width of the chimneys, and convective transport of solute modifying the distribution of solid within the layer. Many assumptions and approximations were made in the analysis in order to arrive at as simple a system of equations as possible. More specific details, such as the proper variation of the mean conductivity of the mushy layer for example, need to be included in the theory before it can be used to make quantitative predictions. The model presented here should, nevertheless, provide a framework to guide and interpret future experimental and theoretical investigations.

This work was developed while I was at the Department of Applied Mathematics and Theoretical Physics of Cambridge University being funded by a research fellowship from Trinity College. I am grateful for this support and for many discussions with A. C. Fowler, H. E. Huppert and R. C. Kerr that helped to shape my ideas. I would also like to thank them, S. H. Davis and A. W. Woods for their helpful criticisms of earlier drafts of the manuscript.

Appendix A

The diameter of the chimneys in a convecting mushy layer is set by thermodynamic balances in the boundary layer around the chimney. The chimney is maintained, in the steady state, by internal dissolution of the dendrites as dilute interstitial fluid is convected from below. When $\mathscr{C}$ is large, the dominant balance in (3.1*b*) for the conservation of solute is

$$\mathscr{C}\frac{\partial \phi}{\partial z} = \boldsymbol{U}\cdot\boldsymbol{\nabla}\Theta. \tag{A 1}$$

At leading order, when $R_m \gg 1$, this can be written as

$$\mathscr{C}\frac{\partial \phi}{\partial z} = U\frac{\partial \theta_1}{\partial r} + W\theta_0'(z). \tag{A 2}$$

Near the wall of the chimney, $\partial\phi/\partial z$ is positive, since the dendrites are dissolving there. The horizontal advective flux $U\,\partial\theta_1/\partial r$ is negative near the wall of the chimney, while the vertical flux $W\theta_0'(z)$ is positive there if the vertical flow W is positive (upwards). Thus the dissolution of dendrites is caused by the vertical advection of solvent and retarded by the horizontal motion of interstitial fluid towards the cooler chimney, which causes deposition of solvent.

If the horizontal transport is weak then the simple balance

$$\mathscr{C}\frac{\partial \phi}{\partial z} \sim W\theta_0'(z) \tag{A 3}$$

applies, which implies that $W = O(1)$ in the boundary layer near the wall of the chimney. Since $W \sim R_m \psi_a \ln\epsilon$, from (5.10), this leads to the scalings presented in (5.11).

With these scalings, the horizontal-advection term

$$\begin{aligned} U\frac{\partial \theta_1}{\partial r} &\sim \left(\frac{\psi_a'}{a}\right)\left(\frac{\psi_a\,\theta_0'}{a}\right) \\ &\sim \epsilon^6 R_c^2 \\ &\sim \left[\frac{R_c}{(R_m \ln\epsilon)^3}\right]^{\frac{1}{2}}, \end{aligned} \tag{A 4}$$

which has been derived from (5.7), (5.8) and (5.11*a*). Thus the horizontal advection is indeed negligible to leading order provided $R_c \ll (R_m \ln\epsilon)^3$ with ϵ given by (5.11*a*).

Once $R_c \gg (R_m \ln\epsilon)^3$, all three terms in (A 2) must balance. In particular, the advective terms balance to give

$$W \sim \epsilon^6 R_c^2, \tag{A 5}$$

which combines with (5.10) to give the scalings presented in (5.12).

Finally, since the balance (A 3) must still apply, we see that

$$\frac{\partial \phi}{\partial z} \sim W \sim \frac{(R_m \ln \epsilon)^3}{R_c} \ll 1 \tag{A 6}$$

with these scalings. The wall of the chimney is defined by

$$\phi(a(z), z) = 0, \tag{A 7}$$

which yields

$$a'(z)\frac{\partial \phi}{\partial r} + \frac{\partial \phi}{\partial z} = 0 \tag{A 8}$$

when differentiated with respect to z. Thus

$$\frac{a'(z)}{a} \sim \frac{\partial \phi}{\partial z} \ll 1, \tag{A 9}$$

which shows that, with the scalings given by (5.12), the walls of the chimney are vertical to leading order.

Appendix B

We wish to determine the volume flux ψ_a through a chimney using (5.5*b*) and (5.5*c*) together with the boundary conditions

$$\psi = 0, \quad \frac{\partial}{\partial r}\left(\frac{1}{r}\frac{\partial \psi}{\partial r}\right) = 0 \quad (r = 0), \tag{B 1}$$

$$\Theta = \theta_0, \quad \frac{\partial \psi}{\partial r} = 0 \quad (r = a), \tag{B 2}$$

$$\Theta = -1, \quad \psi = 0 \quad (z = 0). \tag{B 3}$$

Equation (5.5*b*) expresses the fact that Θ is constant along streamlines, so that $\Theta = \Theta(\psi)$. We use this fact, together with the boundary conditions (B 1)–(B 3), to show additionally that

$$\Theta = -1, \quad \frac{\partial \Theta}{\partial r} = 0, \quad \frac{\partial}{\partial r}\left(\frac{1}{r}\frac{\partial \Theta}{\partial r}\right) = 0 \quad (r = 0), \tag{B 4}$$

$$\frac{\partial \Theta}{\partial r} = 0 \quad (r = a). \tag{B 5}$$

The approximate technique we shall use is a type of Polhausen method, suggested by Lighthill (1953) for solving the laminar, convective flow in tubes. This approach to finding the flow through chimneys was proposed by Roberts & Loper (1983), though they simply set up the appropriate equations without solving them. Here, we consider a simpler problem by ignoring inertia within the chimney and are therefore able to find complete approximate solutions. The method begins by introducing a trial function for the concentration field

$$1 + \Theta = (1 + \theta_0)\{P_1(x) + \mu P_2(x)\}, \tag{B 6}$$

where $x = r/a$, μ is a parameter that must be determined, and the polynomials P_1 and P_2 are given by

$$P_1(x) = 2x^2 - x^4 \tag{B 7}$$

and $$P_2(x) = x^2(1-x^2)^2. \tag{B 8}$$

These are convenient, low-order polynomials that satisfy the boundary conditions (B 1)–(B 5). The trial function (B 6) is used in (5.5*c*), which can be integrated directly to obtain the stream function ψ. Equivalently, we write

$$\psi = a^4 R_C(1+\theta_0)\{\lambda P_1(x)+\lambda_2 P_2(x)+\lambda_3 P_3(x)+\lambda_4 P_4(x)\} \tag{B 9}$$

in terms of the polynomials $P_1(x)$, $P_2(x)$,

$$P_3(x) = x^2(1-x^2)^3, \quad P_4(x) = x^2(1-x^2)^4, \tag{B 10}$$

and differentiate to determine the constants

$$\lambda = \tfrac{1}{32}-\tfrac{1}{160}\mu, \quad \lambda_2 = \tfrac{1}{96}-\tfrac{1}{960}\mu, \quad \lambda = \tfrac{1}{288}+\tfrac{1}{1440}\mu, \quad \lambda_4 = \tfrac{1}{640}\mu, \tag{B 11}$$

from (5.5*c*) and (B 6). Note that the value of the stream function at $r = a$ is

$$\psi_a = \lambda a^4 R_C(1+\theta_0). \tag{B 12}$$

A first approximation to λ could be obtained simply by using the trial function given by setting $\mu = 0$ in (B 6). This would give $\lambda \approx \frac{1}{32} \approx 0.03125$. A better approximation for λ is obtained by choosing μ so that the trial functions satisfy the integral constraint

$$\frac{\mathrm{d}}{\mathrm{d}z}\int_0^a \frac{\partial\psi}{\partial r}(1+\Theta)\,\mathrm{d}r = (1+\theta_0)\,\psi'_a, \tag{B 13}$$

which is derived from (5.5*b*). Substitution of the trial functions given by (B 6) and (B 9) into the constraint (B 13) leads to the quadratic equation for μ,

$$\mu^2 - \tfrac{2992}{617}\mu + \tfrac{1624}{3085} = 0, \tag{B 14}$$

which has roots $\mu \approx 0.111$ and $\mu \approx 4.738$. The larger of these roots corresponds to a flow that reverses within the chimney and has a negative shear at the wall. There is in fact an infinite family of solutions to the full problem given by (5.5*b*) and (5.5*c*) with boundary conditions (B 1)–(B 3) (Lighthill 1953). Our trial functions have identified just two members of the family, and we choose the solution corresponding to $\mu \approx 0.111$, which has no reversals of the flow field, as seeming the most likely to occur. Thus we determine

$$\lambda \approx 0.0306 \tag{B 15}$$

from (B 11).

REFERENCES

Batchelor, G. K. 1974 Transport properties of two-phase materials with random structure. *Ann. Rev. Fluid Mech.* **6**, 227–255.

Chen, F. & Chen, C. F. 1988 Onset of finger convection in a horizontal porous layer underlying a fluid layer. *Trans. ASMEC: J. Heat Transfer* **110**, 403–407.

Copley, S. M., Giamei, A. F., Johnson, S. M. & Hornbecker, M. F. 1970 The origin of freckles in unidirectionally solidified castings. *Metall. Trans.* **1**, 2193–2204.

Fearn, D. R., Loper, D. E. & Roberts, P. H. 1981 Structure of the Earth's inner core. *Nature* **292**, 232–233.

Flemings, M. C. 1981 Process modeling. In *Modeling of Casting and Welding Processes* (ed. H. D. Brody & D. Arpelian), pp. 533–548. Metallurgical Society, AIME.

Fowler, A. C. 1985 The formation of freckles in binary alloys. *IMA J. Appl. Maths* **35**, 159–174.

Hills, R. N., Loper, D. E. & Roberts, P. H. 1983 A thermodynamically consistent model of a mushy zone. *Q. J. Mech. Appl. Maths* **36**, 505–539.

HOWARD, L. N. 1966 Convection at high Rayleigh number. *Proc. Eleventh Intl Congress Applied Mechanics, Münich* (ed. H. Görtler), pp. 1109–1115. Springer.

HUPPERT, H. E. & WORSTER, M. G. 1985 Dynamic solidification of a binary melt. *Nature* **314**, 703–707.

HURLE, D. T. J., JAKEMAN, E. & WHEELER, A. A. 1983 Hydrodynamic stability of the melt during solidification of a binary alloy. *Phys. Fluids* **26**, 624–626.

KERR, R. C., WOODS, A. W., WORSTER, M. G. & HUPPERT, H. E. 1989 Disequilibrium and macrosegregation during solidification of a binary melt. *Nature* **340**, 357–362.

KERR, R. C., WOODS, A. W., WORSTER, M. G. & HUPPERT, H. E. 1990*a* Solidification of an alloy cooled from above. Part 1. Equilibrium growth. *J. Fluid Mech.* **216**, 323–342.

KERR, R. C., WOODS, A. W., WORSTER, M. G. & HUPPERT, H. E. 1990*b* Solidification of an alloy cooled from above. Part 2. Non-equilibrium interfacial kinetics. *J. Fluid Mech.* **217**, 331–348.

KERR, R. C., WOODS, A. W., WORSTER, M. G. & HUPPERT, H. E. 1990*c* Solidification of an alloy cooled from above. Part 3. Compositional stratification within the solid. *J. Fluid Mech.* **218**, 337–354.

LIGHTHILL, M. J. 1953 Theoretical considerations on free convection in tubes. *Q. J. Mech. Appl. Maths* **6**, 398–439.

LOPER, D. E. 1983 Structure of the inner core boundary. *Geophys. Astrophys. Fluid Dyn.* **25**, 139–155.

ROBERTS, P. H. & LOPER, D. E. 1983 Towards a theory of the structure and evolution of a dendrite layer. In *Stellar and Planetary Magnetism* (ed. A. M. Soward), pp. 329–349. Gordon & Breach.

SARAZIN, J. R. & HELLAWELL, A. 1988 Channel formation in Pb–Sn and Pb–Sn–Sb alloy ingots and comparison with the system NH_4Cl–H_2O. *Metall. Trans.* **19a**, 1861–1871.

TAIT, S. & JAUPART, C. 1989 Compositional convection in viscous melts. *Nature* **338**, 571–574.

TURNER, J. S. 1979 *Buoyancy Effects in Fluids*. Cambridge University Press.

TURNER, J. S., HUPPERT, H. E. & SPARKS, R. S. J. 1986 Komatiites II: experimental and theoretical investigations of post-emplacement cooling and crystallization. *J. Petrol.* **27**, 397–437.

WOODS, A. W. & HUPPERT, H. E. 1989 The growth of compositionally stratified solid by cooling a binary alloy from below. *J. Fluid Mech.* **199**, 29–53.

WORSTER, M. G. 1986 Solidification of an alloy from a cooled boundary. *J. Fluid Mech.* **167**, 481–501.